Korean J. Chem. Eng., **31**(1), 142-154 (2014)
DOI: 10.1007/s11814-013-0204-7

pISSN: 0256-1115
eISSN: 1975-7220

Adsorption of Cr (VI) on synthetic hematite (α-Fe_2O_3) nanoparticles of different morphologies

Haleemat Iyabode Adegoke*,†, Folahan AmooAdekola*, Olalekan Siyanbola Fatoki, and Bhekumusa Jabulani Ximba****

*Department of Chemistry, Faculty of Science, University of Ilorin, P.M.B. 1515, Ilorin, Nigeria
**Department of Chemistry, Faculty of Applied Sciences, Cape Peninsula University of Technology, P. O. Box 652, Cape Town, South Africa
(*Received 19 June 2013 • accepted 7 October 2013*)

Abstract−The adsorption of Cr (VI) from aqueous solution onto nanoparticles hematite (α-Fe_2O_3) of different morphologies synthesized by acid hydrolysis, transformation of ferrihydrite, sol gel methods has been investigated. The hematite particle sizes were in the range 15.69-85.84 nm and exhibiting different morphologies such as hexagonal, plate-like, nano-cubes, sub-rounded and spherical. The maximum adsorption capacity of Cr (VI) was found to be in the range 6.33-200 mgg^{-1} for all hematite samples. The kinetics of sorption was rapid, reaching equilibrium at 45-240 minutes. Sorption kinetics and equilibria followed pseudo-second order and Langmuir adsorption isotherm models. The rate constants were in the range 0.996-2.37×10^{-2} g/mg/min for all samples. The maximum adsorption was attained at pH 3.0, while adsorption decreased as the pH increased from pH 3.0 to 10.0. The study revealed that the hematite with plate-like morphology has the highest adsorption capacity. The sorption process has been found to be feasible following a chemisorption process, and adsorption of Cr (VI) onto hematite nanoparticles was by inner sphere surface complexation due to low desorption efficiency in the range 9.54-53.4%. However, the result of ionic strength revealed that the reaction was by outer sphere complexation. This study showed that morphologies play a vital role in the adsorption capacities of samples of hematite in the removal of Cr (VI) from aqueous solution.

Keywords: Hematite Nanoparticles, Morphologies, Chromium, Sorption Capacity, Kinetics

INTRODUCTION

The contamination of water bodies caused by heavy metals is a serious environmental problem because of their toxicity to many life forms [1]. Cr (VI) usually occurs as highly soluble and toxic chromate anions ($HCrO_4^-$ or $Cr_2O_7^{2-}$), which are suspected carcinogens and mutagens [2]. Potable waters containing more than 0.05 mg/L of Cr (VI) are considered toxic [3]. Cr (VI) exerts toxic effects on biological systems.

Chromates are released into the environment by a number of industrial processes, including electroplating, tanning, pulp production and ore and petroleum refining [4].

The different methods for removing metal ions from water and wastewaters include sorption, chemical precipitation, solvent extraction, ion exchange, complexation, filtration and membrane processes. Among these, sorption is a proven technology for the removal of trace contaminants from water [5,6].

Hematite ($\propto$-Fe_2O_3) is a type of iron oxide which crystallizes in the rhombohedral system, space group $R\bar{3}C$. Its crystal structure consists of Fe^{3+} cations octahedrally coordinated by hexagonal close-packed oxygen atoms, the arrangement belonging to the corundum ($\propto$-Al_2O_3) structure type [7,8]. The color is steel grey, blood red in thin fragment, and streak and powder is rouge red; hardness is 6 on Mohs scale and specific gravity is 5.25. The mineral is only weakly magnetic [8]. It is easily obtained by the oxidation of iron in solution followed by heating the precipitate; by oxidation of magnetite, $Fe^{2+}Fe_2^{3+}O_4$; by the dehydration of goethite and by oxidation of ferrous chloride sublimates.

Recent studies have shown that natural hematite has strong affinity for Cr (VI) in aqueous solution [9,10]. Ajouyed et al. investigated the adsorption of Cr (VI) onto commercial macroporous hematite as a function of pH, ionic strength, and initial metal ion concentration [11]. However, according to literature survey, some aspects related to the adsorption of Cr (VI) onto synthetic nanoporous hematite have not been totally elucidated.

The aim of this work is to examine the Cr (VI) ion adsorption behavior from aqueous solution onto different synthetic nanoparticle hematite ($\propto$-Fe_2O_3) prepared in the laboratory by batch method as a function of initial pH of solution, ionic strength, adsorbent dose, initial metal ion concentration and temperature. These hematite samples, though present in the environment, are not of high purity. They are present as mixtures; this necessitates the need to prepare nanostructured hematite of high purity and different morphologies in order to establish optimal conditions for adsorption behaviour of Cr (VI) on the synthetic samples. Adsorption isotherms such as Langmuir, Freundlich, Dubinin-Radushkevich and Temkin isotherms were employed to understand the nature of sorption. This study falls under the context of the treatment of chromium contaminated sites by application of synthetic nanoparticle hematite samples for the remediation of metals in a polluted or contaminated environment.

†To whom correspondence should be addressed.
E-mail: adegoke.hi@unilorin.edu.ng, ihalimat@yahoo.com

EXPERIMENTAL WORK

1. Materials

Hematite of different morphologies was prepared by four different methods. All reagents used in this work were of analytical grade. The hematite samples were prepared from $Fe(NO_3)_3$ (Sigma-Aldrich, 99%), $FeCl_3 \cdot 4H_2O$ (Sigma-Aldrich, 99%), The stock solutions of Cr (VI) prepared from $K_2Cr_2O_7$ (Sigma-Aldrich, 99.9%), HCl (Merck), HNO_3 (Merck) $NaNO_3$ (Sigma-Aldrich, 99%) were also used.

All glassware and polyethylene materials were previously treated for 24 hours in 10% (v : v) nitric acid and rinsed with deionized water (Milli-Q 18.2 MΩ cm^{-1} resistivity).

2. Preparation of Hematite Samples

Five samples of hematite of different morphologies were prepared in the laboratory by four different methods: acid hydrolysis, acid hydrolysis with base addition, sol gel and transformation of ferrihydrite methods. The samples were tagged Ade 1, Ade 2, Ade 3, Ade 4 and Ade 5.

Sample Ade 1 was synthesized by a method similar to the acid hydrolysis method of Schwertmann and Cornell [12] This was prepared by heating 2 L of 0.002 M HNO_3 and 16.6 g of Fe $(NO_3)_3 \cdot 9H_2O$ (0.02 M Fe) at 98 °C with vigorous stirring for 20 minutes. The mixture was then aged for seven days at 98 °C. Sample Ade 2 was synthesized by a modified method of Raming et al. [13]; the particles were obtained by vigorously mixing $FeCl_3 \cdot 6H_2O$ in 2 L of 0.002 M HCl at 98 °C for 15 minutes on a hot plate and later placed in the oven at 98 °C for 48 hours. Sample Ade 3 was prepared by sol-gel method by employing the method of Sugimoto et al. [14]. The particle was prepared by adding 100 ml of 2.0 M $FeCl_3$ slowly into a well stirred 100 ml of 5.4 M NaOH aqueous solution in a 250 ml pyrex flask. The mixture was stirred for 15 minutes and the flask containing a red mixture was placed in an oven at 100 °C for eight days. Sample Ade 4 was prepared by transformation of ferrihydrite method by using the method of Schwertmann and Cornell [12]. Ferrihydrite was precipitated by adding 300 ml 1 M KOH preheated to 90 °C to 40 g of Fe $(NO_3)_3 \cdot 9H_2O$ in 500 ml deionized water preheated to 90 °C, shortly 50 ml of IM $NaHCO_3$, preheated to 90 °C was added to the brown voluminous precipitate and the suspension (pH 8-9) in a closed polyethylene flask was held at 90 °C for 48 hours. Acid hydrolysis using base addition was employed for the preparation of sample Ade 5, and this was done by heating 500 ml of 0.2 M Fe $(NO_3)_3$ prepared at pH 8. The suspension was held at 98 °C for seven days [12].

The precipitate was washed several times with milliQ water (18.2 MΩ resistivity) by dialysis to remove the nitrate and chloride ions, filtered by Millipore glass membrane vacuum filtration system and then oven dried at 40 °C. These products were tagged Ade 1, Ade 2, Ade 3, Ade 4 and Ade 5.

3. Characterization of Sample

The synthesized samples were characterized by physico-chemical methods such as bulk density, pH, point of zero charge, micropore volume and surface area.

The pH of the hematite suspension in water was determined using 1 : 10 mass/volume (hematite-water) mixture ratio with a pH meter (pHS-25 model) [15]. The bulk density of the hematite was determined by Archimedes' principle [16]. The point of zero charge (pzc) of the samples was determined by using mass titration [17] and potentiometric methods. Surface area, micropore volume and micropore area of the hematite samples were determined by BET Nitrogen adsorption and desorption isotherms at liquid nitrogen temperature (77 K) using TRISTAR 3000 Surface area analyzer. 0.3 g of each sample was degassed in N_2 at 77 K for 18 hours prior to measurements.

The synthesized hematite samples were further characterized using X-ray diffraction (PW3050/60 Goniometer), X-ray fluorescence (PAnalytical XPert Pro MPD), Infra-red (Perkin Elmer FT-IR Spectrometer 1000), Scanning electron microscopy (Leo 1430VP and FEI Nova NanoSEM 230) and Transmission electron microscopy (Technai $G^2$20 high resolution transmission electron microscope).

4. Batch Adsorption Studies

4-1. Preparation of Chromium (VI) Stock Solution

Chromium (VI) stock solution of 1,000 mg/L was prepared by dissolving 0.2827 g of $K_2Cr_2O_7$ (Sigma-Aldrich, ≥98.0%) in 100 ml of milliQ water (Resistivity 18.2 MΩ) [18]. Various standard concentrations (1-100 mg/L) Cr (VI) were prepared from the stock by serial dilution and the pH of each standard was adjusted to pH 3 by adding 1.0 to 5.0 ml of 0.1 M trioxonitrate (V) acid (HNO_3) because Cr (VI) predominates at pH 3 as either $HCrO_4^-$ or $Cr_2O_7^{2-}$ as observed from the speciation diagram of chromium. The determinations of the various standard concentrations were determined on an atomic absorption spectrophotometer (Perkin Elmer 3300) at a wavelength of 357.9 nm and at a slit width of 0.7 nm.

4-2. Adsorption of Chromium (VI) on the Prepared Hematite Samples

The various hematite samples (20 mg) were contacted with an initial chromium (VI) concentration of (1 to 100 mg/L) at pH 3, equilibrated on an orbital shaker (GEFRAN 600 model) for 240 minutes at 298 K. The mixture was filtered and analyzed on a UV-Visible spectrophotometer (Aquamate model) at a wavelength of 346 nm [19] or on an atomic absorption spectrophotometer (Perkin Elmer 3300). Adsorption capacity of Cr (VI) was measured and calculated from the difference between initial and final concentration of chromium. The amount adsorbed (mg/g) was calculated using the formula:

$$Q = \frac{V(C_i - C_f)}{W}$$

where Q=Quantity of solute adsorbed from solution of volume, v cm^3

C_i=Initial concentration before adsorption and

C_f=Concentration after adsorption

V=volume of the adsorbate used in L

W=mass of the adsorbent in g

Influence of Some Physicochemical Parameters on Sorption

The influence of initial concentration, ionic strength, pH, temperature and adsorbent dosage was studied on the interaction of oxyanions on each hematite prepared.

5. Sorption Kinetics for Cr (VI) Adsorption

The kinetics study was carried out at pH 3 for Cr (VI) on hematite samples at 20 mg/L equilibrium concentration of Cr (VI). 20 mg of each iron oxide was contacted with 20 ml of 20 mg/L concentration. The mixtures were agitated on an orbital shaker at different time intervals (15 to 240 minutes). After shaking, the samples were

withdrawn at time intervals and filtered. The filtrates were analyzed by UV-Visible spectrophotometer at wavelength of 346 nm or atomic absorption spectrophotometer (Perkin Elmer 3300). The equilibrium time was determined from the graph of amount of solute adsorbed per gram of hematite versus time of contact.

6. Desorption Studies on Cr (VI) Loaded Hematite Samples

Desorption experiment was performed to explore the feasibility of recovering the metals and reuse of the metal-loaded adsorbent (hematite) for further cycle of sorption. The studies were carried out on samples of Cr (VI) loaded hematite with 0.1 M hydrochloric acid and nitric acid as the desorption solutions. To determine the most effective desorption solution, 20 mg of each sample and 20 ml of desorption solution (without any pH adjustment) were kept in contact and agitated on an orbital shaker at 75 rpm and 25 °C for 120 minutes (samples Ade 1, Ade 2, Ade 3, Ade 5) and 240 minutes for Ade 4. The mixture was filtered after desorption and the filtrate analyzed for residual concentration of Cr (VI) by UV-visible spectrophotometer. The desorption efficiency was defined as the ratio of the desorbed amount to the initial adsorbed amount of the respective anions [20]. The desorption efficiency for each adsorbent was determined by dividing amount of chromate ions desorbed by the amount of chromate ions adsorbed in the batch experiments [21].

RESULTS AND DISCUSSION

1. Results of Characterization Studies

1-1. Physico-chemical Characteristics

Physico-chemical characteristics of the synthesized hematite samples are presented in Table 1. The color of the synthesized hematite samples (Ade 1 to Ade 5) ranges from red to reddish brown. This is in line with the color reported by different researchers for synthetic and natural hematite samples [12-13,18]. The pH of the synthesized samples Ade 1 to 5 ranges from 6.65 to 9.06. Samples Ade 1 and 2 had their pH tend a bit towards acidic range; this could be attributed to the method of synthesis, which is hydrolysis, and this involves elimination of few protons into solution. The point of zero charge of the samples ranges from 7.20 to 9.35. The point of zero charge of material facilitates the choice of an adsorbent for removal of certain solutes from waste water; it also makes it possible to predict the pH effect on the phenomena and processes involving adsorption [22]. Sample Ade 4 prepared from transformation of ferrihydrite has the highest value of 9.35. The points of zero charge of the samples were in the range of values reported by Kosmulski [22]. The textures of all the synthesized particles are all fine irrespective of the method of synthesis. The bulk densities of the samples ranged from 0.840 to 1.857 g/cm^3 with sample Ade 3 having the highest density, showing that Ade 3 is the heaviest while Ade 1 is the lightest. The percentage yield for the samples Ade 1-Ade 5 ranged from 62.4 to 98.3% with sample Ade 5 having the highest yield percent and Ade 1 having the lowest yield percent.

Surface area and micropore volume are the key factors in determining whether the material is suitable for the removal of metal ion from aqueous solutions. In addition, the nature of the adsorbent-adsorbate interaction must also be considered. It is understood that the pore volume contributed to the accommodation of metal ion on the adsorbent [23]. From Table 1, the surface area of samples ranged from 26.69 to 52.3 m^2/g with sample Ade 5 having the lowest value of 26.69 m^2/g and Ade 1 having the highest value of 52.3 m^2/g. The surface areas of the samples are comparable with some of the commercial, synthetic and natural iron oxides reported in literature [21]. The micropore volume is in the range 0.00004-0.01078 cm^3/g with (Ade 3) having the highest micropore volume of 0.01078 cm^3/g. It is evident that Ade 1 will have high adsorption capability when compared with other samples. The method of preparation has greatly influenced the surface area of the samples. Schwertmann and Cornell [12] reported values of synthetic hematite in the range 20-90 m^2/g depending on the method of preparation. The micropore area is also in the range of 0.0387 and 21.9537 m^2/g. Sample Ade 3 has the highest micropore area.

1-2. XRD Result

The analysis of hematite samples by x-ray diffraction enables us to determine the crystal phases of the samples. The characteristic reflection peaks (d - values) were matched with data sites for hematite crystalline phases. The recorded indexed diffraction patterns are shown in Figs. 1(a)-(d) where sharp peaks can be observed, as expected for a highly crystalline sample. The positions of all maxima coincided with the peaks characteristics of the hematite phase (JCPDS card 33 - 0664). No diffraction line corresponding to other phases was observed, indicating a high purity of the sample, which is in line with the report of some researchers [7,18,24,25].

The results of x-ray fluorescence (XRF) technique showed that the synthetic iron oxides are mainly hematite. The percentage Fe_2O_3 present for Ade 1 to Ade 4 is in the range 95.29% to 95.42%. This result complements the result obtained from the x-ray diffraction patterns which showed the presence of crystalline hematite from the peaks.

2. Infrared Analysis of the Synthesized Iron Oxides

The surface functional groups were characterized by Fourier transform infrared (FT-IR) spectroscopy. The FTIR spectra of the iron oxide samples are shown in Fig. 2. Table 2 shows the FTIR spectra

Table 1. Physicochemical-characteristics of hematite samples

Samples	Colour	pH	Bulk density (g/cm^3)	PZC	Texture	% Yield	Surface area (m^2/g)	Micropore volume (cm^3/g)×10^{-3}	Micropore area (m^2/g)	External surface area (m^2/g)
Ade 1	Reddish brown	6.75	0.840	7.63	Fine	62.4	52.3±0.4	2.40	4.3477	56.67
Ade 2	Reddish brown	6.65	1.184	7.30	Fine	83.1	31.0±0.2	0.20	0.6127	30.39
Ade 3	Red	7.47	1.857	7.50	Fine	91.7	36.6±0.1	10.78	21.9537	14.65
Ade 4	Reddish brown	9.06	1.417	9.35	Fine	81.3	45.3±0.3	0.04	0.0387	45.34
Ade 5	Reddish brown	7.32	1.201	7.20	Fine	98.3	26.69±0.1	0.88	2.6316	26.07

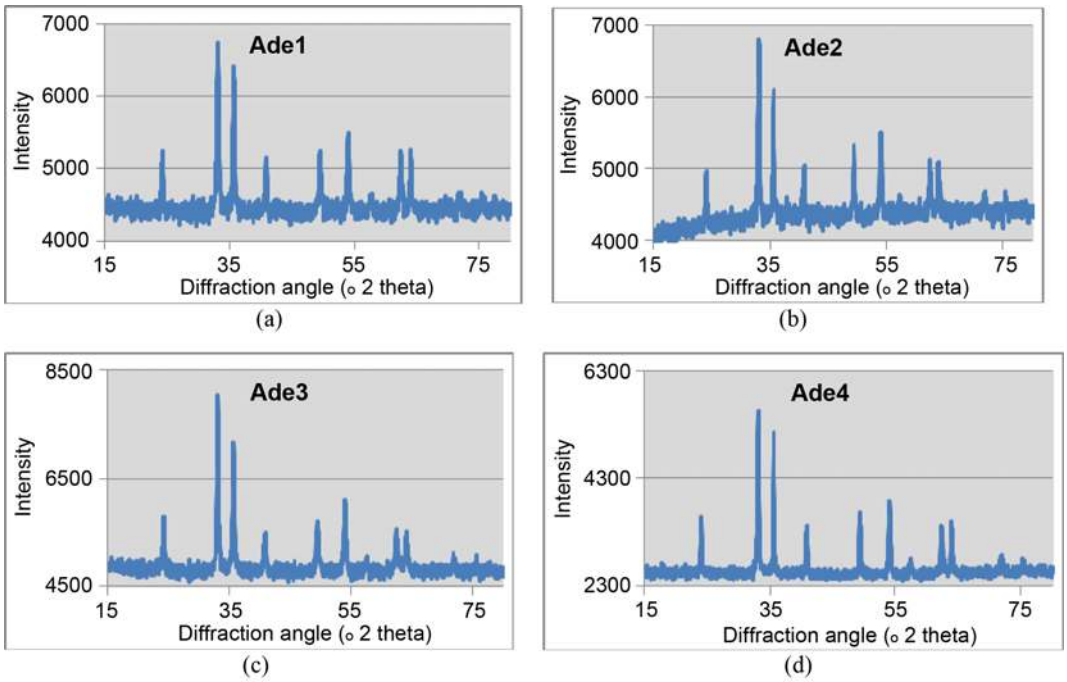

Fig. 1. (a) XRD pattern of hematite Ade1, (b) XRD pattern of hematite Ade2, (c) XRD pattern of hematite Ade3, (d) XRD pattern of hematite Ade4.

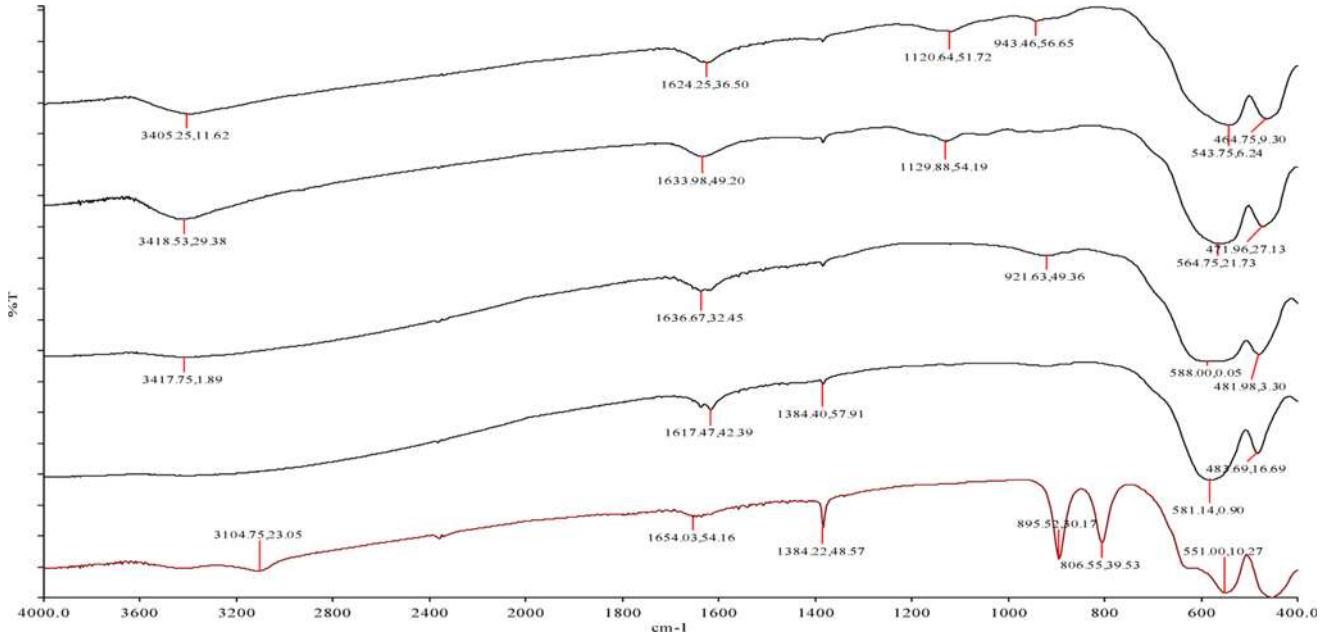

Fig. 2. Fourier transform infrared spectra of Hematite Ade 1-5.

between 4,000 to 400 cm^{-1} of five different hematite samples, Ade 1-Ade 5. The FT-IR spectra of samples show broad bands at 464.75-483.69 and 543.75 cm^{-1}-588 cm^{-1}; these can be attributed to the Fe-O bond vibration of the Fe_2O_3 [26]. The bands at 1,617.25 cm^{-1}-1,654.03 cm^{-1} are assigned to the bending mode of H_2O molecules [27]. The bands at 3,104.25 cm^{-1}-3,421.65 cm^{-1} are assigned to the O-H stretching vibration of absorbed water [24,28]. Hematite spheres have been reported to show IR bands at 575, 485, 385 and 360 cm^{-1} [29]. The band at 921.63 cm^{-1} in Ade 3 spectrum is assigned to O-H deformation.

3. Scanning Electron Microscopy

The SEM micrograph confirms that the synthesized pure hematite samples consist of particles exhibiting different morphological shapes such as plate-like, hexagonal and needle-like. They also contain many pores. The morphology of hematite synthesized by different methods revealed by SEM observation showed an appreciable difference in shape and size of samples. All previous analyses have confirmed that these samples contain hematite as single phases. The

Table 2. Infrared (IR) Frequencies (cm^{-1}) for the synthetic iron oxides

Ade 1	Ade 2	Ade 3	Ade 4	Ade 5	Ade6	Ade7	Assignment
3405.25	3418.53	3417.75	-	3104.75	-	3421.65	O-H stretch vibration of H_2O
1624.25	1633.98	1636.67	1617.47	1654.03	-	1636.33	H-OH bending mode
1120.64	1129.88	-	-	-	-	-	Fe-OH hydroxo complexes
-	-	-	1384.40	1384.22	-	1384.38	O-H deformation
943.46	921.63	-	-	-	-	-	O-H deformation
-	-	-	-	895.52	-	891.84	Fe-OH
543.75	564.75	588.00	581.14	551.00	578.00	-	Fe-O bond vibration
464.75	471.96	481.98	483.69	-	-	-	Fe-O bond vibration

micrographs show that hematite particles are aggregates of small particles. Sample Ade 1 has different agglomerates of particles that are irregular shapes ranging from triangular to plate-like at 100 μm magnification with some degree of porous surface that will aid adsorption. Agglomerates of particles are of spherical shapes at 2 μm magnification, but at 100 μm the morphology ranges from triangular to plate-like to spherical shapes for sample Ade 2. Oval and spherical shapes for sample Ade 3 at 2 μm, while at 20 μm spherical shapes were observed for the same sample. The SEM micrograph for Ade 4 at 2 μm shows agglomeration of particles, while 100 μm magnification shows plate-like shapes. The micrograph of sample Ade 5 revealed it to be spherical at 2 μm magnification, while at 100 μm magnification different irregular shapes ranging from plate-like to triangular were observed.

4. Transmission Electron Microscopy

The transmission electron microscopy (TEM) images of synthesized iron oxide particles are shown in Figs. 3 to 7. The average diameter of particles is between 15.79 nm and 85.84 nm. The TEM micrographs confirm the nanoparticle nature of the synthesized hematite with morphology of the hematite samples ranging from spherical to hexagonal to needle-like depending on the methods of synthesis.

The transmission electron micrographs of the various samples showed that crystallites of the sample had different shapes, such as rod-like, needlelike, hexagonal, spherical shapes and the sizes in the range 15.69-85.84 nm. A high magnification of TEM was also used to further investigate the structure of the hematite types; the micrographs are not shown in this work. The typical TEM images of Ade 1 shown in Fig. 3 reveal that most of the particles were spherical or sub rounded with an average diameter in the range 15.69-39.56 nm. The TEM images of Ade 2 shown in Fig. 4 reveal that most of the particles were sub-rounded with average diameter in the range 52.01-85.84 nm. For sample Ade 3, shown in Fig. 5 irregular shapes such as rod-like, spherical and oval with average diameter in the range 27.86 to 75.01 nm were observed. The TEM images of Ade 4 shown in Fig. 6 reveal that the particles were irregular with nanocube and hexagonal with diameter in the range 26.21-53.59 nm.

The TEM images of Ade 5 shown in Fig. 7 reveal that the particles were nanocubes in shape. The TEM images of all the hematite samples in the range 15.69-36.56 nm confirm the nano-structured nature of the synthesized since sizes are in the range 1 to 100 nm.

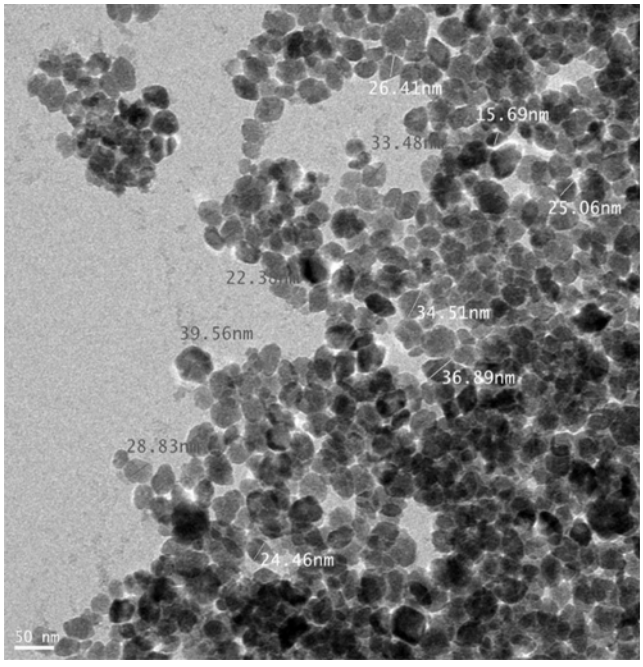

Fig. 3. TEM Micrograph of Ade 1.

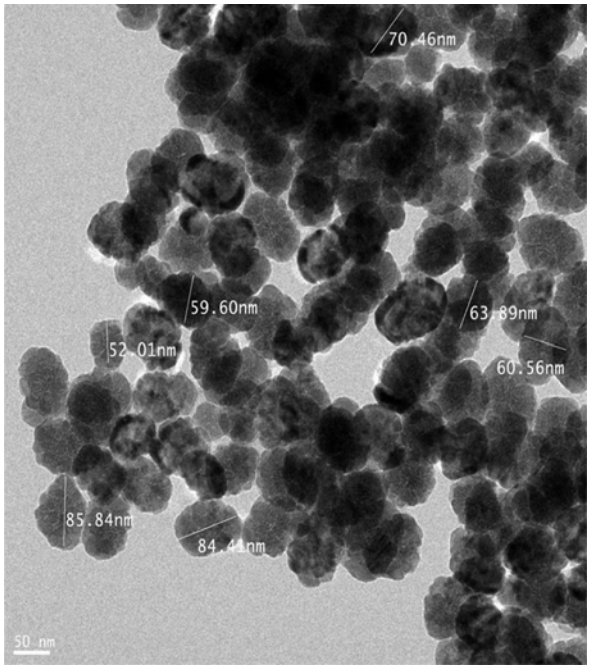

Fig. 4. TEM Micrograph of Ade 2.

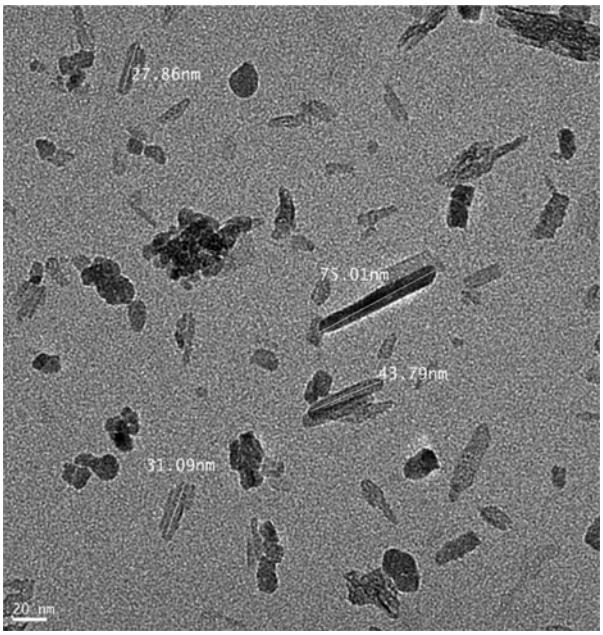

Fig. 5. TEM Micrograph of Ade 3.

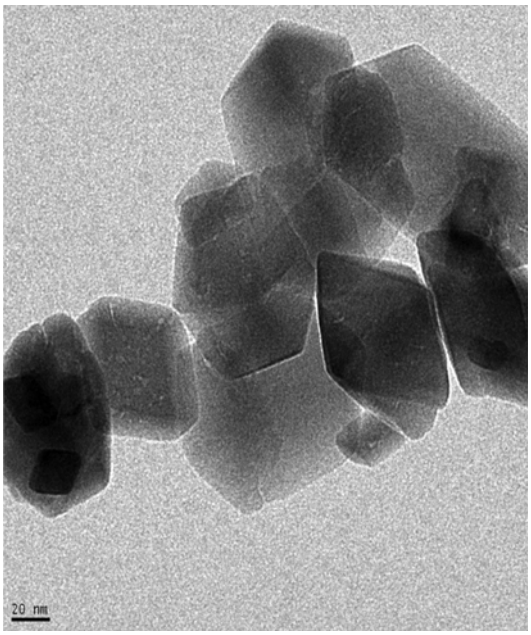

Fig. 7. TEM Micrograph of Ade 5.

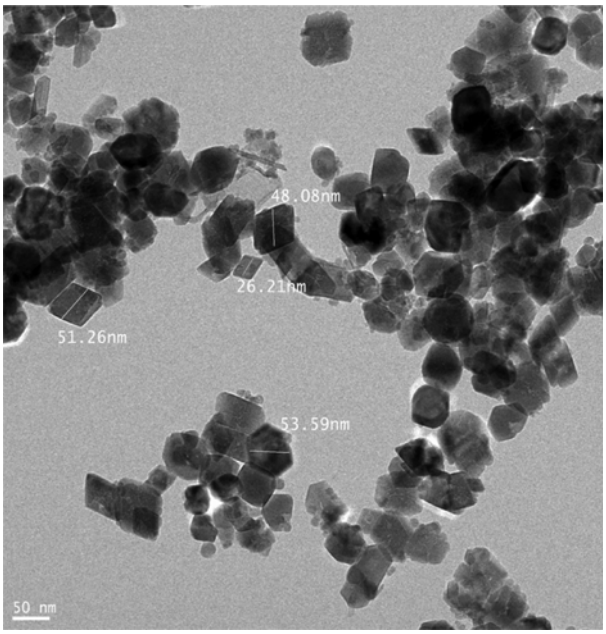

Fig. 6. TEM Micrograph of Ade 4.

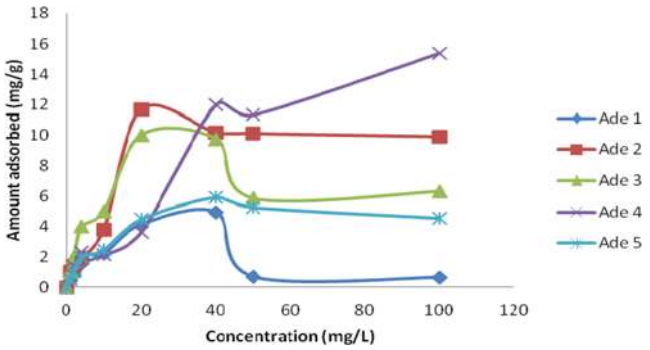

Fig. 8. Effect of Initial Concentration on Adsorption of Cr (VI) onto Ade 1 to Ade 5 at different initial concentration (1 mg/L to 50 mg/L). Stirring rate: 75 rpm, Time: 120 minutes, pH: 3.0 and Temperature: 298 K.

5. Adsorption Studies

5-1. Effect of Initial Concentration of Cr (VI) Ion Solution

20 ml of Cr (VI) ion solution of different concentration ranging from 1 to 100 mg/L was contacted with 20 mg of the adsorbent at a pH of 3.0 at 298 K for 2 hours. The results of the effect of initial concentration of Cr (VI) are shown in Fig. 8. The amount of Cr (VI) ion adsorbed increases with increasing concentration of the adsorbate concentration on the various adsorbents. The maximum amount adsorbed was at 20 mg/L for all the adsorbents with the exception of Ade 2. This could be attributed to the available sites on the surface of the adsorbent. Since the amount of adsorbent used was kept constant for the effect of the initial concentration, the surface of the adsorbent might have been saturated at equilibrium, thereby not accommodating the adsorbate. At this point equilibrium is reached, thereby resisting the uptake of Cr (VI) ion [30]. They exhibited variation in the maximum adsorption capacity. For instance, Ade 3 has the highest capacity for Cr (VI) while Ade 1 has the least. Therefore, 20 mg/L was kept constant for further studies on the effect of various parameters such as pH, time, adsorbent dose, and temperature on adsorption.

5-2. Effect of Time on Adsorption

The adsorption of Cr (VI) on the synthesized hematite (Ade 1-5) as a function of time was investigated under the conditions of adsorbent dose 20 mg, adsorbate concentration 20 mg/L and temperature 298 K. The results of effect of time on adsorption of Cr (VI) on samples Ade 1 to 5 are shown in Fig. 9.

Fig. 9 shows that adsorption of Cr (VI) by the samples Ade 1 to 5 increases with time. The maximum amount adsorbed at different time differs for each adsorbent sample. Samples Ade 2 and Ade 5 had their maximum adsorption capacity within one hour of the experiment; further increase in contact time had no significant effect on

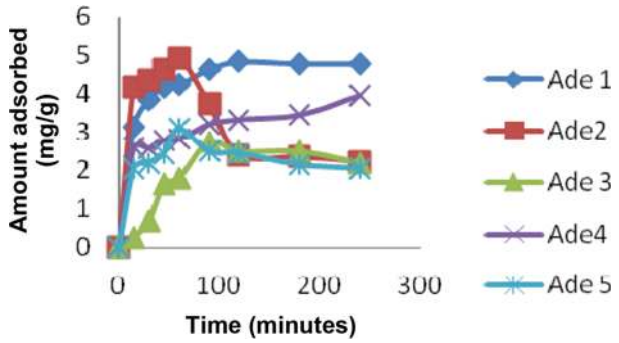

Fig. 9. Effect of contact Time on Adsorption onto Ade 1 to Ade 5 at equilibrium concentration: 20 mg/L. Stirring rate: 75 rpm, pH: 3.0 and Temperature: 298 K.

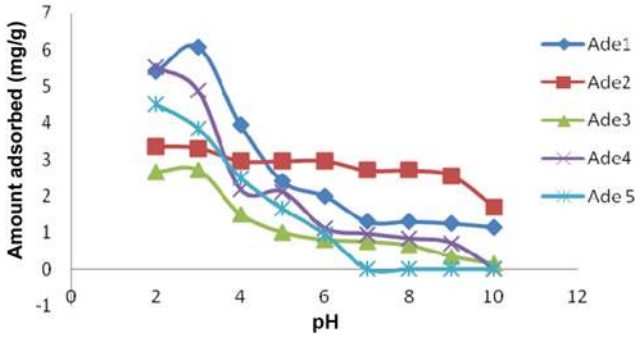

Fig. 10. Effect of pH on the sorption of Cr (VI) onto Ade 1 at equilibrium concentration: 20 mg/L. Stirring rate: 75 rpm, time: 2 hrs and temperature: 298 K.

the adsorption capacity. Ade 1 had its maximum adsorption within 120 minutes of the experiment; Ade 3's maximum adsorption was observed at 180 minutes of contact time. Sample Ade 4 had the highest adsorption within 240 minutes of the experiment. The use of nano-sized particles has advantages of high Cr (VI) adsorption capacity at very short equilibrium time. Similar result was recorded for modified jacobsite magnetic nanoparticles [31].

5-3. Effect of pH on Adsorption

The results of effect of pH on adsorption of Cr (VI) on samples Ade 1 to 5 are presented in Fig. 10. The effect of pH on the removal of Cr (VI) was studied over a pH range 2 to 10. The maximum adsorption was observed between pH 2 and 3 for all samples, while the amount adsorbed decreased as the pH increased. A similar behavior has been reported by different researchers [9,11,32,33] for the uptake of Cr (VI) on various adsorbents. As shown in the Eq. (1) below, hydroxyl species are released from the process of Cr (VI) adsorption instead of hydrogen ions.

$$R+H_2O+HCrO_4^- \leftrightarrow R-HO_3Cr^+ +2OH^- \quad (1)$$

where R represents the adsorbent.

In this case, decreasing the pH will favor the Cr (VI) adsorption on the hematite samples.

At initial pH of 2.0, the adsorbent surfaces might be highly protonated, which favors the uptake of Cr (VI) in the predominant anionic form ($HCrO_4^-$) [34-36]. With increase in pH from 2.0 to 10, the degree of protonation of hematite surfaces reduced gradually, thereby resulting in decrease in the capacity. An increase in pH above 3 shows a slight decrease in adsorption in which the surface of the adsorbent is negatively charged. Decrease in adsorption at higher pH is due to the formation of soluble hydroxyl complexes.

The pH of the system controls the adsorption capacity due to its influence on the surface properties of the adsorbent, and the ionic forms of chromium in solution. The amount of Cr (VI) adsorbed as a function of pH is shown in Fig. 10. Maximum Cr (VI) adsorption occurred at pH 2.0-3.0 for samples Ade 1 to 5. Cr (VI) adsorption decreased as solution pH increased. According to the speciation diagram of Chromium, the dominant form of Cr (VI) at pH 3-6 is $HCrO_4^-$. Increasing the pH will transform the species $HCrO_4^-$ to other form, CrO_4^{2-} [37,38].

Similar observations have also been reported by other authors [39,40]. It can be concluded that the active form of Cr (VI) that can be adsorbed by all adsorbents used in this study is $HCrO_4^-$. At initial pH of 3.0, the adsorbent surfaces might be highly protonated, which favors the uptake of Cr (VI) in the predominant anionic form ($HCrO_4^-$). The two possible reactions are shown in Eqs. (2) and (3):

$$\equiv SOH_2^+ + HCrO_4^- \leftrightarrow SOH_2^+ (HCrO_4^-) \text{ for } pH<pHpzc \quad (2)$$

$$\equiv SOH_2^+ + HCrO_4^- \leftrightarrow SH\ CrO_4 + H_2O \text{ for } pH<pHpzc \quad (3)$$

These mechanisms are in agreement with the findings of previous studies on other adsorbents of different chemical nature [32,37]. The behavior for better adsorption at low pH by these adsorbents may be attributed to the large numbers of H^+ ions present at low pH values which protonate the metal-oxide surface. That results in strong electrostatic attraction between positively charged adsorbent surface and $HCrO_4^-$ leading to higher adsorption. As the pH of the system increases, the number of negatively charged sites increases. A negatively charged surface site on these adsorbents does not favor the adsorption of Cr (VI) due to the electrostatic repulsion. This explains why poor adsorption behavior was observed for $pH>pH_{PZC}$. Furthermore, lower adsorption of Cr (VI) in alkaline medium is also due to the competition from excess OH^- ions with the anions for the adsorption sites [11].

5-4. Effect of Adsorbent Dose on Adsorption of Cr (VI) Ion

The effect of adsorbent dose was studied over an adsorbent dose of 10 mg to 250 mg. Fig. 11 shows the effect of adsorbent dose on adsorption of Cr (VI) on samples Ade1 to Ade 5, and the maximum adsorption was observed at 10 mg for Ade 3, 50 mg for Ade1 and Ade 5, 100 mg for sample Ade 2. Our observation shows that small amount

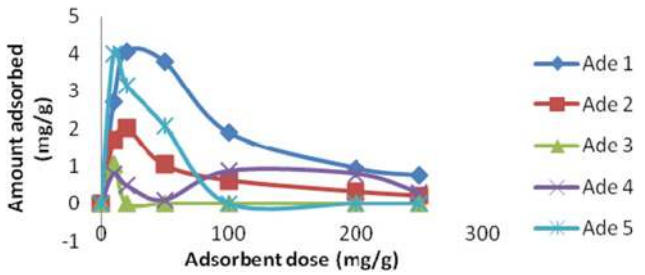

Fig. 11. Effect of adsorbent dose on the sorption of Cr (VI) onto Ade 1 at equilibrium concentration: 20 mg/L. Stirring rate: 75 rpm, time: 2 hrs for Ade 1, 2 and 5, 3 hrs for Ade 3 and 4 hrs for Ade 4 pH: 3.0 and temperature: 298 K.

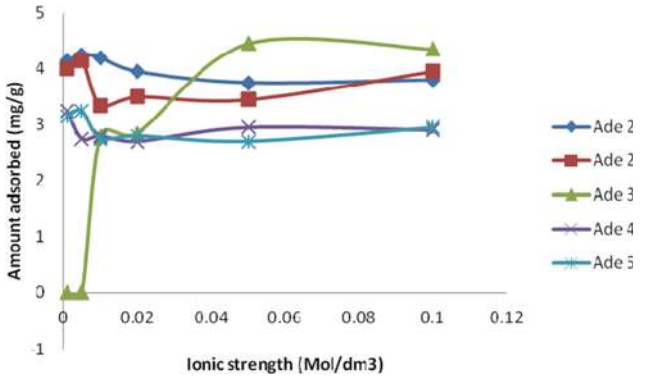

Fig. 12. Effect of ionic strength on Cr (VI) adsorption onto Ade 1-5 at equilibrium concentration: 20 mg/L. Stirring rate: 75 rpm, time: 2 hrs, pH: 3.0, adsorbent dose: 20 mg and temperature: 298 K.

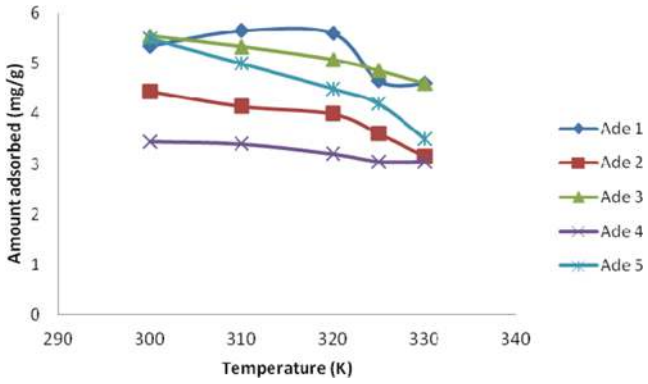

Fig. 13. Effect of temperature on adsorption of Cr (VI) onto Ade 1, Ade 2, Ade 3, Ade 4 and Ade 5 at equilibrium concentration: 20 mg/L. Stirring rate: 75 rpm, time: 2 hrs, pH: 3.0 and adsorbent dose: 20 mg.

of the samples gave maximum adsorption; this is attributed to the high surface area and micropore volume of the nanoparticle material.

5-5. Effect of Ionic Strength on Adsorption of Cr (VI) Ion

Ionic strength is one of the important factors which influence the aqueous phase equilibrium. A number of scientists have intensively investigated this effect. Generally, adsorption decreases with increasing ionic strength of the aqueous solution. The adsorption capacity in this study decreases with increasing ionic strength. Fig. 12 shows the influence of ionic strength at pH 3.0 on the adsorption of Cr (VI) onto hematite samples (Ade 1-5) over an ionic strength range of 0.001 to 0.01 $moldm^{-3}$. The result indicates that Cr (VI) adsorption is dependent on ionic strength for all the hematite samples. For samples Ade 1, 2 and 5 maximum adsorption was observed at ionic strength of 0.005 mol/dm^{-3} $NaNO_3$ while maximum adsorption was observed at 0.05 mol/dm^{-3} for sample Ade 3. The ionic strength can influence the double layer thickness and interface potential, thereby affecting the binding of the adsorbed species. Outer sphere complexes are expected to be more susceptible to ionic strength variations than inner sphere complexes, since background electrolyte ions are placed in the same plane of outer sphere complexes. The study of ionic strength effect on sorption at solid/aqueous interface can be used to indirectly distinguish between the formation of outer-sphere and inner complexes [41]. In general, the sorption mechanism of surface complexation is significantly affected by pH, whereas sorption mechanism of ion exchange is influenced by ionic strength. The strong pH dependence and ionic strength dependence on adsorption of Cr (VI) to hematite samples suggest that the adsorption of Cr (VI) is mainly dominated by both ion exchange and surface complexation.

If sorption is considered as an ion exchange, the reaction between the surface site ≡S-OH and the ions $HCrO_4^-$ can be expressed with the following Eq. (4):

$$\equiv S\text{-}OH + H^+ + HCrO_4^- \leftrightarrow S\text{-}HCrO_4 + H_2O \quad (4)$$

This result is in agreement with the findings of previous studies by other authors [36].

5-6. Effect of Temperature on Adsorption of Cr (VI) Ion

The results of effect of temperature on adsorption of Cr (VI) ion on Ade 1 to Ade 5 are presented in Fig. 13. The adsorption of Cr (VI) decreased with increase in temperature for all samples. The effect of temperature on adsorption of Cr (VI) on hematite samples shows that adsorption decreases with increase in temperature. This indicates the exothermic nature of the adsorption process.

5-7. Adsorption Thermodynamic Studies

The thermodynamics for the adsorption of Cr (VI) on iron oxides was investigated in the range 300-330 K and the influence of temperature on the adsorption under the optimized conditions was studied. There is a little decrease for the equilibrium adsorption capacity with the temperature increase from 300-330 K for all hematite samples (Ade 1-Ade 5) for the adsorption of Cr (VI). Thermodynamic parameters such as change in Gibbs free energy (ΔG), enthalpy (ΔH) and entropy ΔS were determined using the following equation [42].

$$K_c = Q_e / C_e \quad (5)$$

$$\mathrm{Log}K_c = \frac{-\Delta H}{2.303RT} + \frac{\Delta S}{2.303R} \quad (6)$$

$$\Delta G = \Delta H - T\Delta S \quad (7)$$

where K_c is the distribution coefficient, Q_e (mg/g) and C_e (mg/L) are the adsorption capacity and Cr (VI) concentration at equilibrium, respectively.

T is the temperature in Kelvin and R is the gas constant, ΔH and ΔS were obtained from the slope and intercept of the plots of log K_c versus 1/4. Table 3 shows the thermodynamic adsorption parameters ΔH, ΔS and ΔG computed from the plots of log K_c versus 1/T

The negative value of ΔH in the range (−101.4 and −5.67 kJ/mol) for samples Ade 2 to Ade 5 confirms the exothermic adsorption of the Cr (VI) ion.

The negative values of ΔS indicate that there is a decrease in the randomness in solid/solution interface during the adsorption process. The values of ΔG were positive and in the range 0.478-10.6 $kJmol^{-1}$ for sample Ade 2 to 5 for Cr (VI) adsorption The negative values

Table 3. Thermodynamic parameters for the adsorption of Cr (VI) onto hematite samples

Sample	ΔH $kJmol^{-1}$	ΔS $kJmol^{-1}K^{-1}$	ΔG $kJmol^{-1}$
Ade 2	−14.9	−0.0569	2.06
Ade 3	−101.4	−0.376	10.6
Ade 4	−32.6	−0.111	0.478
Ade 5	−5.67	−0.0299	3.24

of enthalpy change (ΔH) and entropy change (ΔS) show that the adsorption process is exothermic in nature.

6. Adsorption Isotherms

6-1. Langmuir Isotherm

The Langmuir isotherm model assumes monolayer adsorption on a uniform surface with a finite number of adsorption sites [38,43]. Once a site is filled, no further sorption can take place at that site. As such the surface will eventually reach a saturation point where the maximum adsorption of the surface will be achieved. The linear form of Langmuir isotherm model is given by the following equation:

$$\frac{C_e}{q_e} = \frac{1}{K_L q_m} + \frac{C_e}{Q} \tag{8}$$

C_e (mg/L) is the concentration of adsorbate left in solution at equilibrium, K_L is the Langmuir bonding energy, q_m (mg/g) is the adsorption maximum (mg/g) and q_e (mg/g) is the amount of adsorbate adsorbed per unit mass of adsorbent.

6-2. Freundlich Isotherm

The Freundlich isotherm is applicable to both monolayer (chemisorption) and multilayer adsorption (physisorption) and is based on the assumption that the adsorbate adsorbs onto the heterogeneous surface of the adsorbent. The empirical Freundlich equation based on sorption onto a heterogeneous surface [44,45] is given below by Eq. (9):

$$q_e = K_f (C_e)^{\frac{1}{n}} \tag{9}$$

where K_f (mg/g) and n are the Freundlich constants K_f and n are indicators of adsorption capacity and adsorption intensity, respectively.

6-3. Temkin Isotherm

The Temkin isotherm model assumes that the adsorption energy decreases linearly with the surface coverage due to adsorbent-adsorbate interactions. The Temkin isotherm equation applied for isotherm analysis is in the following form:

$$q_e = A + B \log C_e \tag{10}$$

According to Temkin Isotherm [46], the linear form can be expressed by equation

$$q_e = \frac{RT}{b} \ln K_T + \frac{RT}{b} \ln C_e \tag{11}$$

where RT/b=B (J/mol), which is Temkin constant related to heat of sorption, whereas K_T (L/g) represents the equilibrium binding energy, R (8.314 J/mol/K) is the universal gas constant at T^0 (k) which is absolute solution temperature.

6-4. Dubinin Radushkevich (D-R) Isotherm

The D-R isotherm model is a semi-empirical equation where adsorption follows a pore filling mechanism. It assumes that the adsorption has a multilayer character, involves van der Waals forces and is applicable for physical adsorption processes. The Dubinin Radushkevich (D-R) isotherm model is more general than the Langmuir isotherm since it does not have the restriction of surface properties or constant sorption potential. It is valid at low concentration ranges and can be used to describe adsorption on both homogenous and heterogeneous surfaces [47]. It has the general expression:

$$q = q_{max} \exp(-\beta \varepsilon^2) - \tag{12}$$

or in the linear form:

$$\ln q = \ln q_{max} - \beta \varepsilon^2 \tag{13}$$

where β is the activity coefficient relating to mean sorption energy (mol^2/kg^2) and ε is the Polanyi potential which is equal to:

$$\varepsilon = RT \ln\left(1 + \frac{1}{C_e}\right) \tag{14}$$

where R is ideal gas constant (8.314 J(mol/K), T is the absolute temperature (k) in Kelvin.

E (Kj/mol) is defined as the free energy change which requires to transfer 1 mol of Cr (VI) from solution to the adsorbent surfaces. The relation is as follows:

$$E = \frac{1}{\sqrt{2\beta}} \tag{15}$$

The exponential data for Cr (VI) sorption onto iron oxides were fitted with Langmuir, Freundlich, Temkin, and Dubinin-Radushkevich models.

The magnitude of the n in the Freundlich isotherm expression shows an indication of favorability of adsorption. Values of n larger than 1 show the favorable nature of adsorption. The values of n (Table 4) suggest that Cr (VI) are favorably adsorbed by iron oxides. The results of the adsorption maxima (Q(mg/g)) from the Langmuir adsorption isotherm suggest that hematite Ade 3 and Ade 5 were not calculated due to low correlation coefficient (R^2). Ade 4 has the highest adsorption capacity of 200 mg/g. From the isotherm result, the Langmuir adsorption isotherm fitted best for the hematite samples with correlation coefficients in the range (0.839<R<0.930) for Cr (VI) adsorption, The q_m values follow the order Ade 4>Ade 1>Ade 2. The separation factor R_L (0.11-0.38) was less than 1.0, indicating that the Cr (VI) ion preferred to remain bound to the hematite surface. The Temkin constants relating to heat of sorption (b) and K_T are in the range of 0.337-12.09×10^3 J/mol and 0.106-6.08 for the adsorp-

Table 4. Adsorption isotherm constants and parameters calculated for Cr (VI) Adsorption

Adsorbents	Langmuir coefficients			Freundlich coefficients			Temkin coefficients		
	q_m	K_L	R^2	n	K_f	R^2	b×10^3	K_T	R^2
Ade 1	28.6	0.080	0.962	2.46	1.65	0.807	0.774	6.082	0.953
Ade 2	6.33	0.42	0.897	1.40	1.87	0.930	12.09	0.445	0.779
Ade 3	-	-	0.194	1.25	2.23	0.703	11.9	0.252	0.718
Ade 4	200	0.0027	0.956	1.43	1.60	0.805	0.337	1.86	0.916
Ade 5	-	-	0.381	1.06	2.23	0.757	10.9	-	-

Table 5. Adsorption kinetics Constants for Cr (VI) adsorption

	Pseudo-second order			Power function			Elovich		
Samples	(K_2(g/mg min)	q_e	R^2	a_2	b_2	R^2	K_p	b	R^2
Ade 1	2.37×10^{-2}	5.03	0.999	2.66	0.904	0.948	0.864	2.893	0.910
Ade 2	2.16×10^{-2}	2.07	0.981	4.08×10^{7}	−0.942	0.615	10.74	−2.912	0.651
Ade 3	1.43×10^{1}	0.129	0.533	-	-	0.300	-	-	0.012
Ade 4	9.96×10^{-2}	4.27	0.991	1.48×10^{2}	0.377	0.986	0.417	2.418	0.957
Ade 5	6.74×10^{-2}	2.06	0.999	3.84	0.403	0.614	0.905	1.462	0.601

tion of Cr (VI) on the iron oxides, respectively. The Temkin isotherm also describes the isotherm data fairly with correlation coefficients in the range (0.534<R<0.953) for Cr (VI) adsorption. The order of fitting of the present data with the isotherm models is Langmuir> Freundlich>Temkin>D-R for Cr (VI).

The values of R^2 showed that the Langmuir model fits best the adsorption data. This suggests the presence of homogeneous surface sites and that monolayer adsorption is occurring for Cr (VI) adsorption with the exception of samples Ade 3 and Ade 5 with low correlation coefficient.

7. Adsorption Kinetic Modeling

To examine the mechanism of adsorption process such as chemical reaction and mass transfer, a suitable model is needed to analyze the rate data. A number of kinetic models have been described to find a suitable mechanism explanation for solid/liquid adsorption systems. Four kinetic models were used to fit the experimental data for the adsorption process of Cr (VI) on iron oxides.

7-1. Pseudo-first Order Equation

The sorption kinetics may be described by a linear pseudo-first order equation:

$$\log(q_e - q_t) = \log q_e - \left(\frac{k_1}{2.303}\right)t \tag{16}$$

where q_e and q_t are the adsorption capacities (mg/g) at equilibrium and at time, t, respectively. k_1 is the equilibrium rate constant of pseudo-first order adsorption (min^{-1}). The slopes and intercepts of $\log(q_e-q_t)$ versus t are used to determine the first order rate constant k_1 and the amount of metal or oxyanion sorbed at equilibrium q_e.

7-2. Pseudo-second Order

The linear pseudo-first order equation is

$$\frac{t}{q_t} = \left(\frac{1}{k_2 q_e^2}\right) + \left(\frac{1}{q_e}\right)t \tag{17}$$

where q_e and q_t have the same meaning as above, K_2 is the rate constant of pseudo-second order adsorption (g $mg^{-1}min^{-1}$). The slopes and intercepts of t/q_t versus t are used to determine the second order rate constant k_2 and the amount of metal or oxyanion sorbed [42] at equilibrium q_e.

7-3. The Power Function Equation

The adsorption kinetics can also be described by power function equation; it describes rates of adsorption (as in the common Freundlich isotherm model) and chemical reaction (for estimation of reaction orders). The linear power function is:

$$\log q_t = \log K_p + v \log t \tag{18}$$

The plot of ln q_t and ln t should give a linear relationship from which K_p, the rate constant and v can be determined from the slopes and intercept, respectively, where K_p and v are constants [42], q_t the adsorption capacity (mg/g) at time, t.

7-4. The Elovich Equation

The Elovich kinetic model is basically used for chemical adsorption on solid surfaces; the adsorption rate is meant to decrease with an increase in the amount of the adsorbed gas or liquid [42].

$$\frac{1}{\beta}\ln(\alpha\beta) + \frac{1}{\beta}\ln t = a_2 + b_2 \ln t \tag{19}$$

where α the initial sorption rate (mg/g min) and β is related to the extent of surface coverage and activation energy for chemisorption (mg/g) [44]. The Elovich equation describes predominantly chemical adsorption on highly heterogeneous adsorbents, but the equation does not propose any definite mechanism for adsorbate-adsorbent interaction [42]. To simplify the Elovich equation, it is written as: $a_2=1/\beta\, l_n(\alpha\beta)$ and $b_2=1/\beta$.

Simple Elovich

$$q_t = a_2 + b_2\, l_n\, t \tag{20}$$

The estimated kinetic models and related parameters (constants) with linear regression coefficient (R^2) are shown in Table 5.

The kinetic adsorption data for Cr (VI) on hematite samples describe the pseudo-second order model best ($0.583<R^2<0.999$), while the pseudo-first order describes the kinetic data poorly with low correlation coefficients in the range ($0.082<R^2<0.852$).The straight line obtained from the plot of t/q_t versus t showed good agreement of experimental data for Cr (VI) adsorption on iron oxides. This suggests that this sorption system follows a pseudo-second order model which is based on the assumption that the rate-limiting step may be chemical sorption or chemisorption involving valency forces through sharing or exchange of electrons between adsorbent and adsorbate. The slopes and intercepts of the plot of $\log(q_e-q_t)$ versus t were used to determine the first order rate constant k_1 and the amount of Cr (VI) sorbed at equilibrium q_e. However, the experimental q_e deviated considerably from the theoretical q_e. This suggests that this adsorption system is not a pseudo-first order reaction. Other models tested describe the kinetic data fairly. The simple Elovich equation explained the kinetic data fairly with correlation coefficient (R^2) for Cr (VI) in the range 0.614 to 0.986 for initial Cr (VI) load of 20 mg/L. This also implies that the sorption is a chemical reaction when compared to the report of some authors [42]. The power function kinetic model equation describes the kinetic data fairly with correlation coefficient in the range 0.601 to 0.957 for Cr (VI) ion on the synthetic iron oxides. The rate of power function v was found to be in the range 0.417 to 0.960 for some of iron oxide type, which

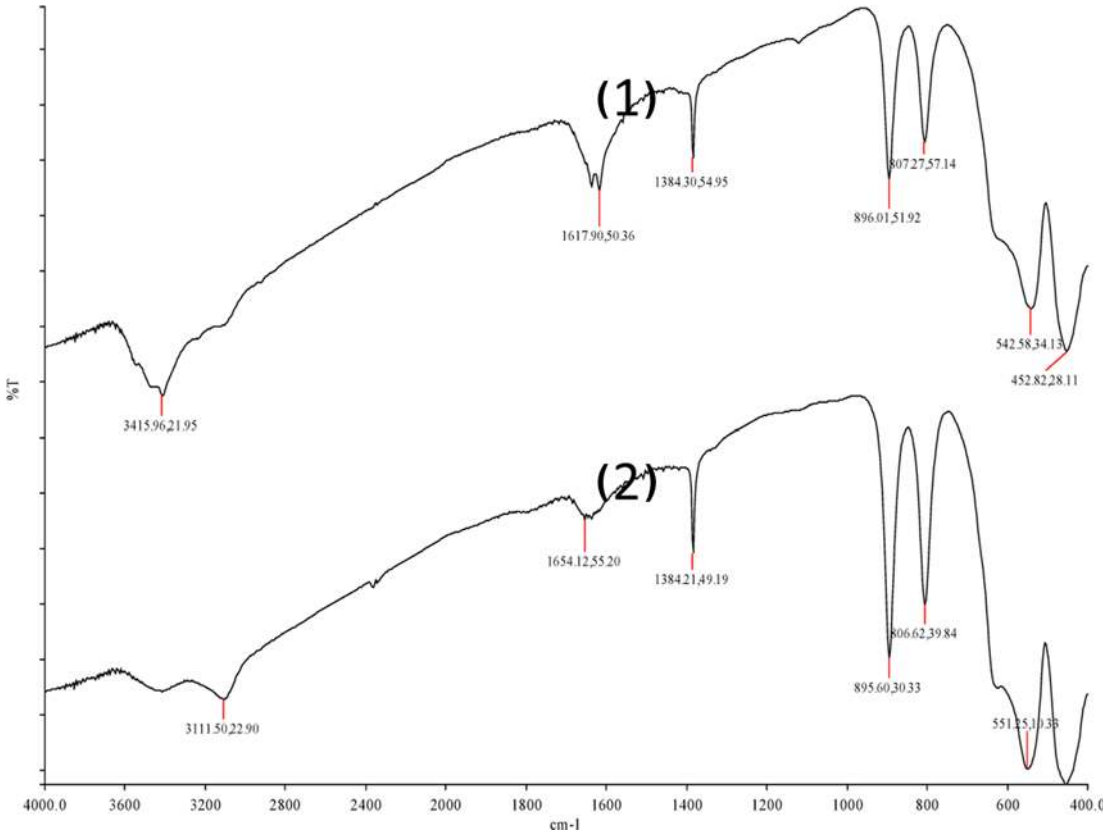

Fig. 14. FT-IR Spectrum of Ade 5 - Cr. After sorption (1), before sorption (2).

indicates that the power function model described the time-dependent of Cr (VI) on iron oxides as the value of constant v was less than 1. This observation is supported by the observation of some researchers [42,45]. However, no systematic order is found for fitting the kinetic data with analyzed model equations, as the present kinetic data were found to fit best the pseudo-second order model.

8. IR Spectra of Samples after Cr (VI) Adsorption

A shift of absorption bands should occur if the symmetry of the ion is lowered by interaction with hydrous iron oxide. Chromate interacts with iron oxide surface by chemical bonding as indicated by a comparison of the spectra before and after sorption of chromate. Hsia et al. [48] reported the adsorption of chromate at absorption band 934.3 cm^{-1}, which was not observed in the original spectrum of iron oxide. Chromate absorption bands are indicated by FT-IR spectra (Fig. 14) data which slightly shift on the spectra of iron oxides, verifying that chromate could specifically adsorb on iron oxide surface. The FTIR spectra of Cr (VI) sorbed hematite Ade 1 expected at 3,405, 1,624, 1,120, 943, 1,384 cm^{-1} had shifted, respectively, to 3,418, 1,617, 536, 455, 564 and 464 cm^{-1} while the peak at 943 cm^{-1} disappeared completely. The bands at 3,418, 1,633, 1,129, 564 and 471 cm^{-1} in sample Ade 2 shifted to 3,419, 1,636, 1,384, 1,126, 554 cm^{-1}, respectively. The band at 471 cm^{-1} remained unchanged after the adsorption of Cr (VI) from aqueous solution.

The spectrum for Ade 3 indicated absorption in the regions 3,417, 1,636, 921, 588 and 481 cm^{-1}. The band between 900 and 778 cm^{-1} was linked to the presence of Cr (VI) during sorption experiment by Pakade et al. [49]; it was also reported by Gourdarzian et al. [50] that bands at 938 and 790 cm^{-1} were attributed to the interaction of Cr (VI) with the adsorbent. Miller and Wilkins [51] also observed chromate anion FTIR bands at 930 and 765 cm^{-1} in polyethylene imine supported silver dichromate oxidizing polymeric reagent. The band at 921 cm^{-1} could be linked to the presence of Cr (VI) attached during the preparation of sample Ade 3; this also complements the result of x-ray fluorescence for the elemental composition of the sample, which revealed 0.56% of Cr_2O_3. The bands at 3,417, 1,636, 588 and 481 cm^{-1} shifted to 3,415, 1,617, 578, 480 cm^{-1} while the band 921 cm^{-1} disappeared completely after adsorption of Cr (VI) from aqueous solution.

Ade 5 - Cr (VI) sorbed showed that the bands at 3,111, 1,654, 1,384, 895, 806 and 551 cm^{-1} shifted to 3,415, 1,617, 1,384, 896, 807, 542 and 452 cm^{-1}, respectively. Specific adsorption is likely to be formed according to the FTIR measurements results at Cr (VI) and hematite interface. This result is in line with the report of Hsia et al. [48] that reported a slight shift on the spectrum of hematite loaded with chromate. It is therefore apparent that chromate could specifically adsorb on hematite surface.

9. Desorption Result

An indication of desorption efficiency for each adsorbent is given in Table 6.

It was also observed that the percentage chromate desorbed was in the range 13.9-33.90% for all hematite types using HCl and lower for HNO_3 values in the range 10.9 to 20.1%. This also supports the result of desorption efficiency. Since over 80% is not displaceable by HNO_3 for hematite samples, it can be concluded that inner-sphere complexes were formed by the chromate anion and hematite samples. The relatively higher value recorded for HCl could be due to

Table 6. % desorbed, desorption efficiencies and desorption index of Chromate from hematite samples

Samples	% Desorbed		% Desorption efficiency		Desorption index	
	HNO_3	HCl	HNO_3	HCl	HNO_3	HCl
Ade 1	17.2	14.3	46	42	1.86	1.72
Ade 2	17.6	11.6	45	35	2.21	1.55
Ade 3	15.8	11.3	32	25	3.16	1.33
Ade 4	14.8	11.1	64	77	2.76	4.26
Ade 5	13.9	12.9	58	55	2.39	2.23

its complexing ability. The FTIR results also complement this result. The bonds of chromate-loaded iron oxides were shifted and the intensity of the bands was higher. These spectroscopic variations suggested the formation of inner-sphere chromate complexes on hematite samples. These desorption experiments thus suggest a strong bond of chromate to the iron oxides. This, in turn, indicates a reaction between the surface complex $\equiv Fe\text{-}OH_2^+$ and $HCrO_4^-$ forming a $\equiv Fe\text{-}O_4HCr$ at the hematite surface (inner sphere).

The desorption index (DI) was calculated for the various hematite types to evaluate the degree of reversibility of the sorption process [52]. DI is the ratio of percentage of metal ion on adsorbent at the end of sorption to the percentage of metal on the adsorbent at the end of desorption. A sorption process is considered to be completely irreversible when DI equals 1. The degree of irreversibility of a sorption process increases as DI value deviates from 1. The result of the desorption index is in the range 1.33 to 3.16 for the various iron oxide types using HCl as the desorption solution, while 1.86-4.26 using HNO_3 as the desorption solution for Cr (VI) loaded-iron oxides. This also complements the observation of inner-sphere complexes formed by Cr (VI) on the oxide types. Table 6 summarizes the desorption indices of iron oxides.

Table 7 shows different adsorbents and their adsorption capacity; it was observed that adsorbents of nanoparticle range exhibit higher adsorption capacity.

CONCLUSIONS

A batch technique was used to study the sorption of Cr (VI) from aqueous solution onto the synthesized iron oxide hematite as a function of pH, contact time, ionic strength, adsorbent dose and temperature. The results indicated that adsorption decreased with increasing pH for Cr (VI) ion. Adsorption data were fitted with Langmuir, Freundlich, Temkin and Dubinin Radushkevich adsorption isotherm model for Cr (VI) ion. The adsorption process was found to depend on the concentration of metal ion, ionic strength, pH, adsorbent dose and temperature. The result of adsorption experiment for Ade 4 was found to have high adsorption capacity when compared with other hematite samples studied with adsorption capacity of 200 mgg^{-1}. The adsorption of Cr (VI) was found to be pH dependent and maximum adsorption observed in the pH range 2-3.

The adsorption isotherm data for Cr (VI) at pH 3.0, respectively, and temperature 25±2 °C fitted the Langmuir adsorption isotherm model best. The result of the adsorption isotherms suggests the presence of homogeneous surface sites and monolayer adsorption for Cr (VI) on the various hematite types. The separation factor calculated from the Langmuir constant also showed that the adsorption process of Cr (VI) is favorable. The result of the isotherms revealed that the reaction is a chemisorption process. The thermodynamic parameters indicated the feasibility and exothermic nature of the adsorption process.

The adsorption kinetic data for Cr (VI) at pH 3.0 at temperature 25±2 °C described the pseudo-second order equation best. The adsorption of Cr (VI) ions reached equilibrium in 4 hours. The sorption of Cr (VI) is dependent on ionic strength at low pH value. The thermodynamic parameters derived from temperature-dependent sorption isotherms suggest that the sorption process of Cr (VI) onto all iron oxide types is spontaneous and exothermic.

Sample Ade 4 showed distinct features among all the five synthesized hematites with adsorption isotherm fitting all the Langmuir, Freundlich and Temkin with correlation co-efficient 0.956, 0.790, 0.916 for Cr (VI) sorption. The adsorption kinetic model for sample Ade 4 fitted three (3) kinetic models tested pseudo-second order, Elovich and power function model. Based on all results, it can be concluded that hematite Ade 1 to Ade 5 are effective nanoparticle adsorbent for the removal of Cr (VI) from wastewaters in terms of their high adsorption capacities.

ACKNOWLEDGEMENTS

Haleemat Iyabode Adegoke wishes to thank the management of University of Ilorin for the Staff Development Award for Ph.D. re-

Table 7. Comparison of Adsorbents for the removal of Cr (VI) from aqueous solution

Adsorbents	pH	Nature	Langmuir		Freundlich		References
			Q (mg/g)	b (L/mg)	K_f (mg/g)	n (L/mg)	
Hematite	8	Macroporous	2.299	0.388	0.544	1.272	[11]
Goethite	8	Macroporous	1.955	0.261	0.348	1.238	[11]
α-Alumina	8	Macroporous	2.158	0.182	0.297	1.175	[11]
Hematite (Ade I)	**3**	**Nanoporous**	**28.6**	**0.080**	**1.65**	**2.46**	**This study**
Hematite (Ade 2)	**3**	**Nanoporous**	**6.33**	**0.42**	**1.40**	**1.87**	**This study**
Hematite (Ade 3)	**3**	**Nanoporous**	**ND**	**ND**	**1.25**	**2.23**	**This study**
Hematite (Ade 4)	**3**	**Nanoporous**	**200**	**0.24**	**1.43**	**1.60**	**This study**
Hematite (Ade 5)	**3**	**Nanoporous**	**ND**	**ND**	**1.06**	**2.23**	**This study**

ND: not determined

search in Chemistry, and the Cape Peninsula University of Technology, South Africa for a 3-month fellowship which greatly assisted in the completion of the work.

REFERENCES

1. B. J Gao, Y. B. Li and Z. P. Chen, *Chem. Eng. J*., **150**, 337 (2009).
2. E. M. N. Chirwa and Y. T. Wang, *Environ. Sci. Technol*., **31**, 1446 (1997).
3. A. Barai and R. D. Engelken, *Environ. Sci. Pollution.*, **5**, 121 (2002).
4. L. E. Eary and D. Rai, *Environ. Sci. Technol*., **22**, 972 (1988).
5. G. L. Ghurye, D. A. Clifford and A. R. Tripp, *J. Am. Water Works Assoc*., **91**, 85 (1999).
6. D. A. Clifford, *Adsorption and ion exchange*, in: F. W. Pontius (Ed.), Water Quality and Treatment: A Handbook of Community Water Supplies, McGraw-Hill, New York, 561 (1990).
7. X. Wang, X. Chen, X. Ma, H. Zheng, M. Ji and Z. Zhang, *Chem. Phys. Lett*., **384**, 391 (2004).
8. McGraw-Hill Encyclopedia of Science and Technology New York, **8**, 185 (2002).
9. D. B. Singh, G. S. Gupta, G. Prasad and D. C. Rupainwar, *J. Environ. Sci. Health*, **A28**, 1813 (1993).
10. G. E. Brown Jr., S. A. Chambers, J. E. Amonette, J. R. Rustad, T. Kendelewicz, C. S. Doyle, D. Grolimund, N. S. Foster-Mills, S. A. Joyce and S. Thevuthasan, *J. Conference Abstract*, **5**, 253 (2000).
11. O. Ajouyed, C. Hurel, M. Ammari, L. Ben Allal and N. Marmier, *J. Hazard. Mater*., **174**, 616 (2010).
12. U. Schwertmann and R. M Cornell, *Iron oxide in the laboratory: preparation and characterization*, Wiley-VCH Weinheim, Germany, 1 (1991).
13. T. P. Raming, A. J. A. Winnubst, C. M. Van Kats and A. P. Philipse, *J. Colloid Interface Sci.*, **249**, 346 (2002).
14. T. Sugimoto, M. M. Khan and A. Muramatsu, *Colloids Surf. A: Physicochem. Eng. Aspects*, **70**, 167 (1993).
15. International Institute of Tropical Agriculture (IITA), Selected Methods for Soil and Plant Analysis. Manual Series, **1**, 3 (1979).
16. B. H. Hameed, R. R. Krishni and S. A. Sata, *J. Hazard. Mater*., **162**, 305 (2009).
17. J. S. Noh and J. Schwarz, *J. Colloid Interface Sci*., **130**, 157 (1989).
18. M. Tadic, N. Citakovic, M. Panyam, Z. Stojanovic, D. Markoviv and V. Spasojevic, *J. Alloys Compds*, **509**, 7639 (2011).
19. H. I. Adegoke and F. A. Adekola, *Colloid J*., **74**, 420 (2012).
20. K. Goh, T. Lim, A. Bana and Z. Dong, *J. Hazard. Mater*., **179**, 818 (2010).
21. Y. Mamindy-Pajany, C. Hurel, N. Marmier and M. Romeo, *Desalination*, **281**, 93 (2011).
22. M. Kosmulski, *J. Colloid Interface Sci*., **253**, 77 (2002).
23. M. V. Subbaiah, G. Yuvaraya, Y. Vijaya and A. Krishnaiah, *J. Taiwan List. Chem. Eng*., **42**, 965 (2011).
24. W. Qin, C. Yang, R. Yi and G. Gao, *J. Nanomaterials*, DOI:10.11555/2011/159259 (2011).
25. L. Wang and L. Gao, *J. Colloid Interface Sci*., **349**, 519 (2010).
26. S. K. Apte, S. D. Naik, R. S. Sonawane and B. B. Kalew, *J. Am. Ceram. Soc*., **90**, 412 (2007).
27. M. Gotic, S. Music, S. Popovic and L. Sekovanic, Croatica, *Chem. Acta*, **81**, 569 (2008).
28. H. D. Ruan, R. I. Frost, J. T. Kloprogge and L. Duong, *Spectrochim. Acta Part A*., **58**, 967 (2000).
29. J. E. Iglesias and C. J. Serna, *Miner. Petrogr. Acta*, **29A**, 363 (1985).
30. K. Simeonidis, S. Tresintsi, C. Martinez-Boubeta, G. Vourlias, I. Tsiaoussis, G. Stavropoulos, M. Mitrakas and M. Angelakeris, *Chem. Eng. J*., **168**, 1008 (2011).
31. J. Hu, I. M. C. Lo and G. Chen, *Langmuir*, **21**, 11173 (2005).
32. J. Fang, Z. Gu, D. Gang, C. Liu, E. S. Ilton and B. Deng, *Environ. Sci*., **44**, 4748 (2007).
33. A. Imai and E. F. Gloyna, *Water Res.*, **24**, 1143 (1990).
34. P. Srinivas, R. Shashikant and G. S. Munjunatha, *J. Environ. Sci. Health*, **A27**, 2227 (1992).
35. A. Ajmal, A. H. Khan, S. Ahmad and A. Ahmad, *Water Res*., **32**, 3085 (1998).
36. B. Yu, Y. H. Zhang, A. Shukla, S. S. Shukla and K. L. Dorris, *J. Hazard. Mater*., **384**, 83 (2001).
37. C. Namasivayam and R. T. Yamuna, *Chemosphere*, **30**, 561 (1995).
38. D. Q. L. Oliveira, M. Goncalves, L. C. A. Oliveira and L. R. G. Guiherme, *J. Hazard. Mater*., **151**, 280 (2008).
39. C. H. Weng, Y. C. Sharma and S. H. Chu, *J. Hazard. Mater.*, **155**, 65 (2008).
40. C. Namasivayam and M. V. Sureshkumar, *Bioresour. Technol*., **99**, 2218 (2008).
41. Y. Arai, E. J. Elzinga and D. L. Sparks, *J. Colloid Interface Sci*., **235**, 80 (2001).
42. N. Ouazen and M. N. Sahmoune, *Int. J. Chem. Rea. Eng. Article*, **A151**, 1 (2010).
43. U. M. Uysal and I. Arai, *J. Hazard. Mater*., **149**, 482 (2007).
44. S. H. Chien and W. R. Clayton, *Sci. Soc. Am. J*., **44**, 265 (1980).
45. S. Basha and Z. V. P. Murthy, *Process Biochem.*, **42**, 1521 (2007).
46. M. I. Temkin and V. Pyzhev, *Acta Physiochemica*, USSR 12, 327 (1940).
47. B. Hu, W. Cheng, H. Zhang and S. Yang, *J. Nucl. Mater*., **406**, 263 (2010b).
48. T. S. Hsia, S. L. Lo, C. F. Lin and D. Y. Lee, *Colloids Surf. A*, **85**, 1 (1994).
49. V. Pakade, E. Cukrowska, J. Darkwa, N. Torto and L. Chimuka, *Water SA*, **37**, 529 (2011).
50. N. Goudarzian, P. Ghahramani and S. Hossini, *Polym. Int*., **36**, 61 (1996).
51. F. A. Miller and C. H. Wilkins, *Anal. Chem*., **24**, 1253 (1952).
52. D. G. Strawn and D. L. Sparks, *Soc. Sci. Soc. Am. J*., **64**, 144 (2000).